THE JOURNAL OF BIOLOGICAL CHEMISTRY VOL. 290, NO. 8, pp. 4856–4865, February 20, 2015

Toxicity of an α-Pore-forming Toxin Depends on the Assembly Mechanism on the Target Membrane as Revealed by Single Molecule Imaging*[S]

Received for publication, July 30, 2014, and in revised form, December 12, 2014 Published, JBC Papers in Press, December 18, 2014, DOI 10.1074/jbc.M114.600676

Yamunadevi Subburaj[‡§], **Uris Ros**[¶], **Eduard Hermann**[‡§‖], **Rudi Tong**[‡], **and Ana J. García-Sáez**[‡§‖1]

From the [‡]*Max Planck Institute for Intelligent Systems, Heisenbergstr. 3, 70569 Stuttgart, Germany, the* [§]*German Cancer Research Center, Bioquant, Im Neuenheimer Feld 267, 69120 Heidelberg, Germany, the* [¶]*Center for Protein Studies, Faculty of Biology, Calle 25 #455, Plaza de la Revolución, La Habana, Cuba, and the* [‖]*Interfaculty Institute of Biochemistry, University of Tübingen, Hoppe-Seyler-Str. 4, 72076 Tübingen, Germany*

Background: Equinatoxin II is a model α-pore-forming toxin that kills cells by porating the host plasma membrane.
Results: On the membrane, equinatoxin II does not adopt a unique oligomeric state, but assembles into multiple coexisting species related to toxicity.
Conclusion: Toxicity of Equinatoxin II depends on its assembly mechanism.
Significance: A new molecular mechanism is proposed for α-pore-forming toxins action.

α-Pore-forming toxins (α-PFTs) are ubiquitous defense tools that kill cells by opening pores in the target cell membrane. Despite their relevance in host/pathogen interactions, very little is known about the pore stoichiometry and assembly pathway leading to membrane permeabilization. Equinatoxin II (EqtII) is a model α-PFT from sea anemone that oligomerizes and forms pores in sphingomyelin-containing membranes. Here, we determined the spatiotemporal organization of EqtII in living cells by single molecule imaging. Surprisingly, we found that on the cell surface EqtII did not organize into a unique oligomeric form. Instead, it existed as a mixture of oligomeric species mostly including monomers, dimers, tetramers, and hexamers. Mathematical modeling based on our data supported a new model in which toxin clustering happened in seconds and proceeded via condensation of EqtII dimer units formed upon monomer association. Furthermore, altering the pathway of EqtII assembly strongly affected its toxic activity, which highlights the relevance of the assembly mechanism on toxicity.

Pore-forming toxins (PFTs)[2] are potent virulence factors widespread in all kingdoms of life (1), like the diphteria or anthrax toxins from bacteria, or perforin, in the mammalian immune system. Their mechanism of action is key to understanding the host/pathogen interactions and for their use in medical applications (2). PFTs perturb the plasma membrane integrity to disrupt ion homeostasis of the host cell or to facilitate the entry of toxic components. They are secreted as soluble proteins and adopt a membrane-inserted conformation on the target membrane. Importantly, toxin oligomerization seems to be a general prerequisite for pore formation. According to the α-helical or β-sheet structure of the membrane-integrated domains, they are classified as α-PFTs or β-PFTs, respectively. The best studied pores are those formed by β-barrels, like α-hemolysin (3) or cholesterol-dependent cytolysins (4). Research lags far behind in the case of α-PFTs, for which the supramolecular organization on the target membrane remains unsettled (5).

Equinatoxin II (EqtII) is a model α-PFT that has proven useful to improve our general understanding of how these toxins work. It is produced by sea anemone *Actinia equina* and belongs to the family of actinoporins. EqtII kills several cell types and has been shown to induce plasma membrane reorganization in the host cell (6). Upon binding to the target membrane, EqtII oligomerizes and inserts its N-terminal α-helix, which forms part of the pore structure (7, 8). Remarkably, membrane lipids also contribute to the rim of the pore (9), giving an estimated size of 2 nm in diameter (10, 11).

There is strong debate regarding the stoichiometry of α-PFTs. Some studies suggest that the toxins of the actinoporin family and Cry1Aa from *Bacillus thuringiensis* form tetramers (12, 13). In contrast, the structures of similar proteins like Cytolysin A and Fragaceatoxin C support pores formed by higher oligomeric species (14, 15). One problem is that most studies with PFTs have been performed under equilibrium conditions using artificial lipid bilayers. The stoichiometry and assembly mechanism of PFTs in the natural context of the target host membrane, as well as the dynamic nature of the oligomerization process leading to cell death, remain largely unexplored.

Here, we visualized individual, fluorescently labeled EqtII molecules on the plasma membrane of living cells by total internal reflection fluorescence (TIRF) microscopy (16, 17). We found that in cells EqtII exists in a dynamic equilibrium of multiple oligomeric species including significant populations of

* This work was supported by the Max Planck Society, the German Cancer Research Center, and Bundesministerium für Bildung und Forschung Grant 0312040 and grants from the EMBO and DAAD (to U. R.).
[S] This article contains supplemental Movie S1.
[1] To whom correspondence should be addressed: Interfaculty Institute of Biochemistry, 72076 Tübingen, Germany. Tel.: 49-7071-29-73318; Fax: 49-7071-29-5070; E-mail: ana.garcia@uni-tuebingen.de.
[2] The abbreviations used are: PFT, pore-forming toxin; EqtII, Equinatoxin II; TIRF, total internal reflection fluorescence; MSD, mean square displacement; ODE, ordinary differential equation.

monomers, dimers, tetramers, and hexamers. Based on our experimental data and on mathematical analysis of the temporal distribution of species, a new model is proposed by which EqtII assembly proceeds via sequential condensation of dimers formed by the association of toxin monomers on the cell surface. Interestingly, a mutant version of EqtII with lowered hemolytic activity followed a distinct oligomerization pathway, which demonstrates the functional relevance of the molecular steps involved in toxin assembly. In contrast to previous models, our data suggest a toxic mechanism by which membrane permeabilization would be simultaneously induced by oligomers of variable stoichiometry.

EXPERIMENTAL PROCEDURES

Cloning, Expression, and Protein Purification and Labeling—*eqtII* gene, introduced in the pET21a$^+$ expression plasmid, was purchased from Entelchon (Bad Abbach, Germany). The EqtII-R126C single mutant was obtained by replacing the corresponding residue by Cys. EqtII wild type and EqtII-R126C were expressed in *Escherichia coli* BL21-RIPL cells and purified by combining cation-exchange chromatography in SP-Sepharose column (GE Healthcare) and gel filtration chromatography in a Superdex 200 HP column (GE Healthcare). The single cysteine mutant of EqtII-L26C, provided by G. Anderluh, was obtained and purified as described in Malovrh *et al.* (27). EqtII-R126C was labeled with Alexa Fluor 488 maleimide (EqtII-Al488), whereas EqtII-L26C was labeled with Alexa Fluor 555 maleimide (EqtII-L26C-Al555) according to the manufacturer's instructions (Invitrogen). The separation of the labeled protein from excess free dye was achieved with a 10DG gel filtration column (Bio-Rad). Labeling efficiency was determined to be 76% (EqtII-R126C) or 86% (EqtII-L26C) by fluorescence spectroscopy with a Specord S100 (Analytik Jena, Jena, Germany).

Hemolytic Assay—The hemolytical activity of wild type EqtII, mutants, and labeled proteins was assessed turbidimetrically at 600 nm by using a microplate reader (Tecan, Crailsheim, Germany). A erythrocyte suspension was prepared using pooled fresh human red blood cells collected intravenously from at least four healthy volunteers. Cells were washed by repeated centrifugation (14,000 $\times$ *g*, 5 min), the cell pellet was resuspended in Tris-buffered saline (TBS: 145 mM NaCl, 10 mM Tris-HCl, pH 7.4) and finally diluted to an apparent absorbance of 0.1. Proteins were 2-fold serially diluted in a flat-bottom 96-well microplates in a final volume of 100 μl of TBS. The hemolysis reaction was started by adding the same volume of red blood cells. Hemolysis was recorded for 10 min with intermittent shaking. The hemolytic activity (HA) was calculated after 5 min as a function of protein concentration as follows:

$$HA_{5min}(\%)\frac{A_0 - A_t}{A_0 - A_{pt}} \times 100 \qquad \text{(Eq. 1)}$$

where A_t, A_0, and A_{pt} represent the absorbance at 5 min, at time 0, and in the presence of an excess of protein, respectively.

Cell Culture—COS1 cells were cultured in DMEM (high glucose; Sigma) with 10% fetal calf serum, 1% antibiotics (penicillin and streptomycin) at 37 °C and in the presence of 5% CO_2. All cells were regularly passaged at subconfluence and plated at 2–5 $\times$ 10^4 cells/ml density. For imaging experiments, the cells were seeded in LabTek chambers (Nunc). Experiments were carried out 24 or 48 h after seeding.

Total Internal Reflection Microscopy—Single molecule images were acquired using a total internal reflection microscope equipped with an EMCCD camera (Andor iXon3 DU-897), a Nikon Apo TIRF $\times$60 oil immersion objective (NA 1.49), and a 561-nm diode laser. The cells were maintained at 37 °C during the whole experiment and imaged in a buffer containing 150 mM NaCl, 20 mm Hepes, pH 7.4, 20 mM trehalose, 15 mM glucose, 5.4 mM KCl, 0.9 mM $MgSO_4$, and 0.5 mM $CaCl_2$. After single cells were selected and focused using bright field, fluorescently labeled EqtII was added. Movies were acquired with an exposure time of 200 ms at different times after toxin addition.

Single Particle Tracking—Particles were detected and tracked using the u-track software (18). The detection parameters used were as follows: psf σ-2.5, integration window-3, and αLocMax-0.2. Tracking was constrained to the particles that were present in at least 10 consecutive frames. The particles detected and tracked were subjected to further analysis using Matlab (Mathworks) and Origin8.5. For each particle trajectory, the two-dimensional mean square displacement (MSD) for every time interval was calculated according to Refs. 19–21,

$$\mathrm{MSD}(t) = \frac{1}{N}\sum_{i=1}^{N}[(X_{i+t} - X_i)^2 + (Y_{i+t} - Y_i)^2] \qquad \text{(Eq. 2)}$$

where N is the number of frames, and X and Y describe the particle position at each frame. The diffusion coefficient was calculated by fitting the data of *MSD versus* time lag (Δ_t) to diffusion models. In case of simple two-dimensional Brownian motion, the *MSD* is related to the diffusion coefficient D by,

$$\mathrm{MSD}(\Delta t) = 4D\Delta t \qquad \text{(Eq. 3)}$$

and for subdiffusion the relationship is given by,

$$MSD(\Delta t) = \langle r_c^2\rangle[1 - A_1\exp(-4A_2D_t/\langle r_c^2\rangle)] \qquad \text{(Eq. 4)}$$

where r_c^2 is the confinement size, and A_1 and A_2 are constants determined by the confined geometry (22).

Calibration of Single Molecule Fluorescence in the TIRF Microscope—To calibrate the fluorescence signal in the TIRF microscope, we acquired movies of single Alexa 488 or Alexa 555 molecules dried on a coverslip under the same conditions as in the cell experiments. The decrease in fluorescence intensity of single photobleaching steps (n = 25) (Fig. 4, *B* and *C*) followed a normal distribution and was fitted with a Gaussian curve that provided the average fluorescence signal of one Alexa 488 or Alexa 555 molecule and the error of the estimation. This value was comparable with that obtained in similar experiments using EqtII labeled with Alexa 488 or Alexa 555 (EqtII-Al488, Eqt-L26C-Al555) dried on a coverslip or in lipid bilayers. Movies were acquired under the same conditions used for cells until all the particles were photobleached. Because EqtII does not diffuse in the lipid bilayers, we observed mostly monomers. Monomer value was used to calculate the fluorescence signal corresponding to dimers, trimers, tetramers, etc.

(Fig. 4*C*) (16). The calibration was repeated prior to every experiment to avoid artifacts due to changes in the microscope setup. Moreover, the brightness of the least bright particle imaged from cells was also comparable.

Stoichiometry Analysis—The individual particles were detected and the fluorescence intensity of each particle was estimated by fitting a two-dimensional Gaussian and averaging from the beginning of the movie until they are photobleached (Fig. 4, *A* and *B*). By fitting a Gaussian curve to the distribution of fluorescence intensities, the mean intensity μ and standard deviation σ of a single fluorophore was calculated. With μ and σ, the fluorescence intensity of N colocalized fluorophores can be given by $\mu_N = N\mu_1 \pm N^{1/2}\,\sigma_1$ (Fig. 4*C*). The number of Gaussians that can be fitted to the distribution of fluorescence intensity was estimated according to Ref. 16 and,

$$N_{\max} = (\mu_1/\sigma_1)^2 \qquad \text{(Eq. 5)}$$

$N_{\max}$ is 4 for our data, so we restricted our fittings to four species in EqtII-L26C-Al555 and calculated the corresponding μ and σ values. In the case of EqtII-Al488 we fitted up to hexamers, but only four species were detected after labeling correction. For determining the stoichiometry of EqtI, ~500 individual particles were detected and analyzed for each time point. As the fluorescence signal of the different species is expected to be the same at all measured times, the distribution of the fluorescence intensity of all the particles at all time points was globally fitted with a sum of four Gaussians using obtained μ and σ values. The Gaussian model used for the fit is given by,

$$\varphi(i) = \sum_{n=1}^{N_{\max}} A_n \times \frac{1}{\sigma\sqrt{2\pi}} e^{-\frac{(i-\mu\cdot n)^2}{2(\sigma\cdot n)^2}} \qquad \text{(Eq. 6)}$$

where $\varphi(i)$ is the frequency of particles having intensity i, n is the component number, and A_n is the area under the curve of component n. The area A under the curve of each component was used to estimate the percentage of occurrence of each species and at each time point as described in Ref. 23. All percentage values mentioned here were corrected considering that 76% of the protein is fluorescent.

Mathematical Simulations—We modeled the kinetics of EqtII oligomerization with a simple model based on mass action kinetics. The system is represented by a set of coupled ordinary differential equations (ODEs) with reaction rate constants used as fitting parameters. Numerical integration and fitting was performed in COPASI 4.11 (24). We estimated the total area concentration of EqtII molecules on the cell surface by counting all the individual particles in a cell, taking into account the stoichiometry of each particle and dividing by the observed membrane area. In the best fit for EqtII-Al488, we obtained a sum of squared residuals of 1.7×10^{-5} [particles/μm^2]^2 ($1.1 \times 10-3$ [particles/μm^2]^2 for EqtII-L26C-Al555). This corresponds to an averaged uncertainty of $1.2 \times 10-3$ particles/μm^2 ($8.3 \times 10-3$ particles/μm^2 for EqtII-L26C-Al555) for each concentration curve.

ODEs for Modeling EqtII Oligomerization—The model for EqtII-Al488 is represented by 4 coupled ODEs originating from mass action kinetics.

$$\frac{dx_1}{dt} = -2k_1x_1^2 + 2k_{-1}x_2 \qquad \text{(Eq. 7)}$$

$$\frac{dx_2}{dt} = k_1x_1^2 - k_{-1}x_2 - 2k_2x_2^2 + 2k_{-2}x_4 - k_3x_2x_4 + k_{-3}x_6 \qquad \text{(Eq. 8)}$$

$$\frac{dx_4}{dt} = k_2x_2^2 - k_{-2}x_4 - k_3x_2x_4 + k_{-3}x_6 \qquad \text{(Eq. 9)}$$

$$\frac{dx_6}{dt} = k_3x_2x_4 - k_{-3}x_6 \qquad \text{(Eq. 10)}$$

The ODEs for EqtII-L26C-Al555 are,

$$\frac{dx_1}{dt} = -2k_1x_1^2 + 2k_{-1}x_2 - k_2x_1x_2 + k_{-2}x_3 - k_3x_1x_3 + k_{-3}x_4 \qquad \text{(Eq. 11)}$$

$$\frac{dx_2}{dt} = k_1x_1^2 - k_{-1}x_2 - k_2x_1x_2 + k_{-2}x_3 - 2k_4x_2^2 + 2k_{-4}x_4 \qquad \text{(Eq. 12)}$$

$$\frac{dx_3}{dt} = k_2x_1x_2 - k_{-2}x_3 - k_3x_1x_3 + k_{-3}x_4 \qquad \text{(Eq. 13)}$$

$$\frac{dx_4}{dt} = k_3x_1x_3 - k_{-3}x_4 + k_4x_2^2 - k_{-4}x_4 \qquad \text{(Eq. 14)}$$

χ_i stands for the concentration of species i (monomers, dimers, trimers, and tetramers). In this model, the total number of monomeric EqtII molecules is conserved.

RESULTS

Design and Activity of the Mutants—For single molecule tracking studies we produced EqtII single cysteine mutants, as wild type EqtII does not possess any Cys. This is essential to know exactly the amount of fluorophores we have per protein molecule. We replaced a single residue at positions 26 or 126 by Cys to obtain two mutants with different activities. Position 126 is located near the C terminus, which is distant from the regions of the proteins involved in membrane binding or pore formation (7, 8). Neither the mutation nor the labeling at position 126 affected protein activity (Fig. 1) as described previously by Anderluh and co-workers (25). Conversely, mutation at position 26 is located in the N-terminal α-helix, which directly participates in pore formation (8). It has been proposed that the EqtII N-terminal α-helix must be inserted prior to oligomerization to allow an efficient pore formation (26). Activity of the EqtII-L26C mutant was dramatically reduced in comparison with the wild type protein, but partially recovered activity when labeled (Fig. 1). Such an effect of labeling on protein activity was also obtained by Malovrh *et al.* (27). As free Alexa 555 does not have hemolytic activity (at least under our experimental conditions), it seems like labeling might induce some conformational change in EqtII-L26C, which allowed repairing the pore-formation ability. Moreover, the activity of EqtII-L26C-Al555 reproduces all the important events described for the wild type (6),

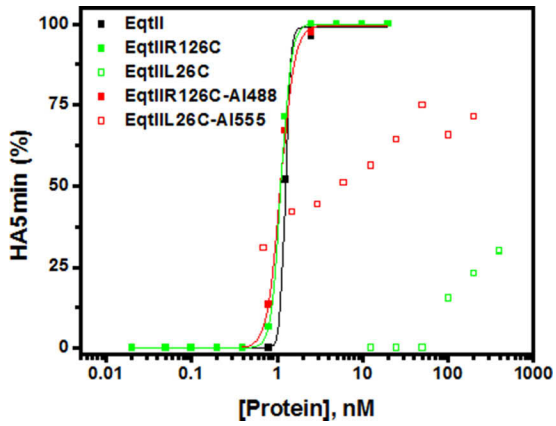

FIGURE 1. **Hemolytic activity of single Cys mutants and labeled EqtII.** Dose dependence analysis of human red blood cell lysis induced by increasing concentrations of the corresponding toxins after a 5-min incubation. The time course of hemolysis was followed by the decrease in turbidity of a cell suspension initially adjusted to an optical density of 0.1 at 600 nm. Experimental conditions: T ~ 22 °C, buffer: TBS, cell concentration: 10^5 cell/ml. Neither free Alexa 488 nor Alexa 555 had hemolytic activity under the experimental conditions.

thus this mutant allowed us to study the oligomerization process with slower kinetics. In the hemolytic assay, each mutant showed the same behavior when changing the dye (Alexa 488 or Alexa 555) (data not shown). Thus we concluded that there is no effect of the dye in toxin aggregation or membrane interaction, which made EqtII-Alexa 488 and EqtII-L26C-Alexa 555 suitable for our study.

Equinatoxin II Particles Show Confined Diffusion on the Plasma Membrane—Upon binding to the target cell, EqtII induces the formation of immobile raft-like domains where the toxin is localized (6). However, the dynamic behavior of the individual EqtII molecules within these domains and on the remaining membrane remains unknown. To investigate the mobility of the individual EqtII particles in the plasma membrane, we performed single molecule tracking experiments. We used EqtII labeled with Alexa 488 at a single Cys introduced at residue 126 (EqtII-Al488) (see "Experimental Procedures"), which retains its hemolytic activity (Fig. 1). Prior to toxin addition, an area containing individual cells was selected and focused using bright field microscopy. Then, we added the fluorescently labeled toxin at a final concentration of 10 nM to COS-1 cells and acquired movies in the TIRF mode. This is the optimal concentration at which we have a significant number of particles and the cell is alive for long enough to follow particle dynamics. Under our experimental conditions, the cells died in a couple of minutes, but was enough to record the toxin diffusion at 1 min. The evanescent wave generated under TIRF illumination ensured that only the molecules bound to the plasma membrane in contact with the coverslip glass were excited (Fig. 2*A*). As the oligomerization kinetic takes place in the time frame of cell death and we observed labeled proteins in the cells surface adhered to the glass, toxin molecules in free solution are able to access such regions of the plasma membrane from the water interface between the adherent cells and the glass, and as a consequence this population can be considered as representative for EqtII effect (28).

Single molecules of EqtII-Al488 appeared as bright spots diffusing in a dark background (Fig. 2*B*). We tracked individual

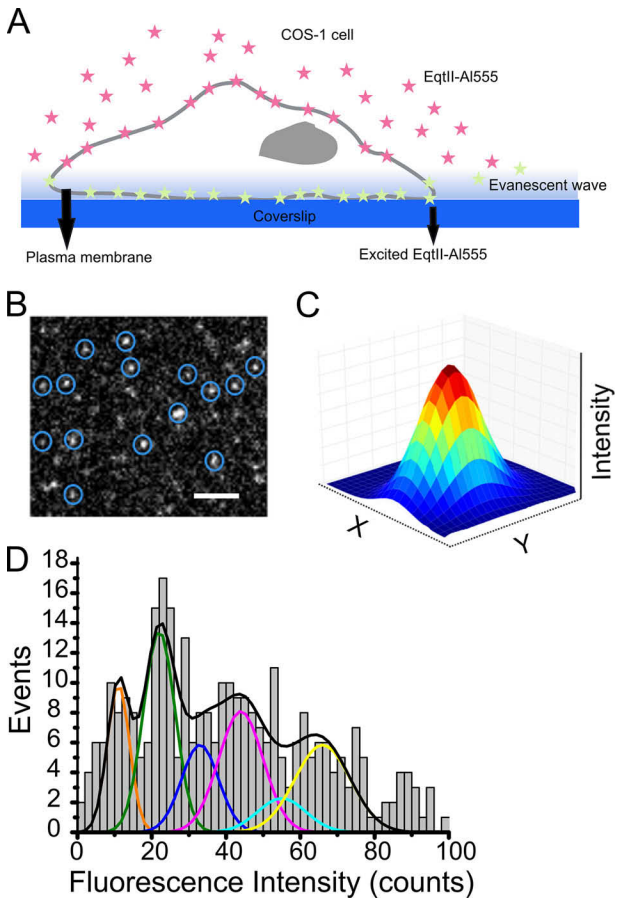

FIGURE 2. **Experimental design.** *A,* upon addition to the extracellular medium, EqtII-Al488 and EqtII-L26C-Al555 bind quickly to the plasma membrane of COS-1 cells. Only a fraction bound to the part of the plasma membrane closer than ~100 nm to the glass coverslip is illuminated in the TIRF setup and emits fluorescence. *B*, single molecules of labeled EqtII in the plasma membrane appear in the images as bright spots and can be detected by image processing (*blue circles*). *C,* the signal of an individual molecule is fitted with a two-dimensional Gaussian curve from which the fluorescence intensity of the molecule is calculated. *D,* by analyzing several hundreds of individual particles, the intensity distribution of labeled EqtII on the cell surface is obtained. To calculate stoichiometry, we fitted the histograms with a sum of Gaussians whose centers and widths correspond to the values calculated for the oligomeric species (Fig. 4). The area of each Gaussian is proportional to the fraction of that species.

particles of EqtII over consecutive images in time-lapse experiments. Fig. 3*A* shows representative trajectories of EqtII-Al488 particles from movies acquired 1 min after toxin addition. The MSD analysis, as well as the histogram of diffusion coefficients, showed that almost all EqtII-Al488 particles exhibited subdiffusion (Fig. 3, *B* and *C*), which fit best to confined diffusion with an averaged *apparent* diffusion coefficient of $0.36 \pm 0.07\ \mu m^2\ s^{-1}$.

On the Cell Surface EqtII Is Present as a Mixture of Multiple Species—To analyze the stoichiometry of single EqtII molecules, we performed a brightness analysis of the individual particles that has been established and successfully used to determine the stoichiometry of other membrane protein complexes, including β-pore-forming toxins (29–31). To this aim, we calibrated the fluorescence signal in the TIRF microscope prior to each experiment (see "Experimental Procedures" and Fig. 4). We characterized the fluorescence signal of EqtII-Al488 monomers via photobleaching analysis and Gaussian fitting to the

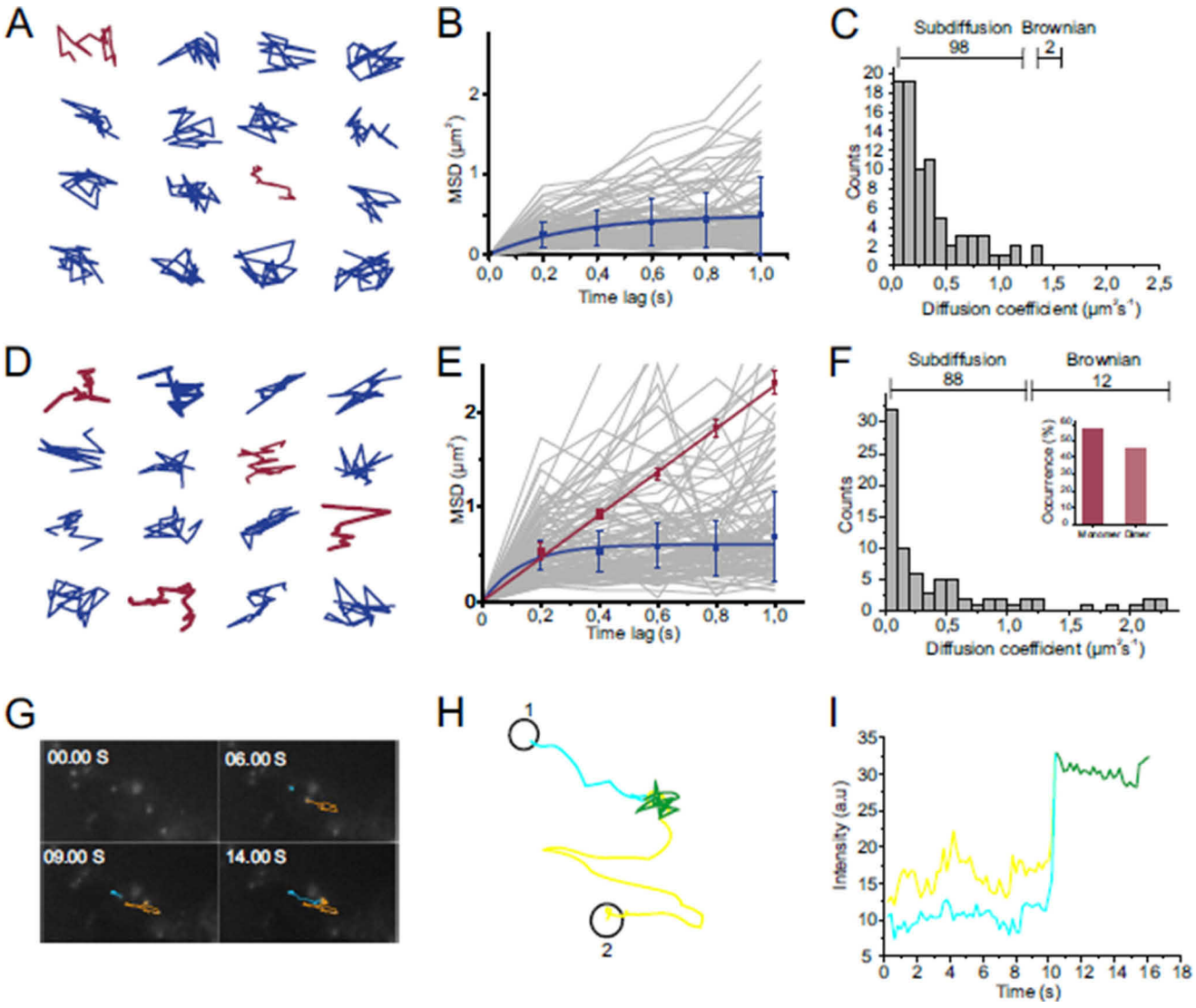

FIGURE 3. **Mobility analysis of EqtII-Al488 and EqtII-L26C-Al555.** *A* and *D,* representative trajectories of individual EqtII-Al488 (*A*) and EqtII-L26C-Al555 (*D*) molecules on the cell surface. Brownian motion is shown in *red* and subdiffusion in *blue*. *B* and *E,* plot of MSD *versus* time lag for 100 EqtII-Al488 (*B*) or EqtII-L26C-Al555 (*E*) (*gray lines*). Averages (including S.D.) for trajectories classified as Brownian (*red*) or as confined (*blue*) are shown. *C* and *F*, distribution of diffusion coefficients *D* of EqtII-Al488 (*C*) and EqtII-L26C-Al555 (*F*). *F*, *inset*, the particles following Brownian diffusion are monomers and dimers. *G,* direct visualization of EqtII-Al488 oligomerization. TIRF images showing two EqtII-L26C-Al555 molecules (*cyan* and *yellow*) forming a stable complex on the cell surface. *Scale bar*, 1 μm. *H*, same traces as in *G*, but the trajectory of complex shown in *green*. *I,* the fluorescence signal of the complex equals the sum of the two individual EqtII-L26C-Al555 particles.

histogram of the distribution of fluorescence intensities measured. Based on these values, we calculated the expected brightness of higher oligomers.

Then, we calculated the brightness of individual EqtII-Al488 particles in the membrane of living COS-1 cells by fitting with a two-dimensional Gaussian (Fig. 2*C*) and plotted the intensity distribution as a histogram (Fig. 2*D*). Visual inspection of the broad distribution of fluorescence intensities indicates the presence of species brighter than monomers. We fitted the histogram of fluorescence intensities with a linear combination of Gaussian curves corresponding to the brightness calculated for the different oligomeric forms (16, 17, 31, 32). These results indicate that EqtII does not exist in the plasma membrane of living cells in a unique oligomeric form, but, surprisingly, as a mixture of oligomeric species.

To investigate the temporal dynamics of EqtII oligomerization, we took images at 10 s, 30 s, and 1 min after adding the fluorescently labeled toxin to COS-1 cells. This is the time frame under which we observed EqtII-Al488-induced cell death. We fitted the histograms of fluorescence intensity distribution measured for ~500 particles at each time point as explained above (Fig. 5, *A*–*C*). The area under each curve was used to calculate the percentage of occurrence of each species, which were then corrected for partial labeling. Due to this correction, the percentages of the different species do not exactly coincide with the area of the respective Gaussians. Our analysis revealed that even 10 s after adding the toxin to the cells (Fig. 5, *D*–*G*) we could observe significant amounts of dimers, tetramers, and hexamers along with similar levels of monomers. A few brighter particles were detected in the image but we did not

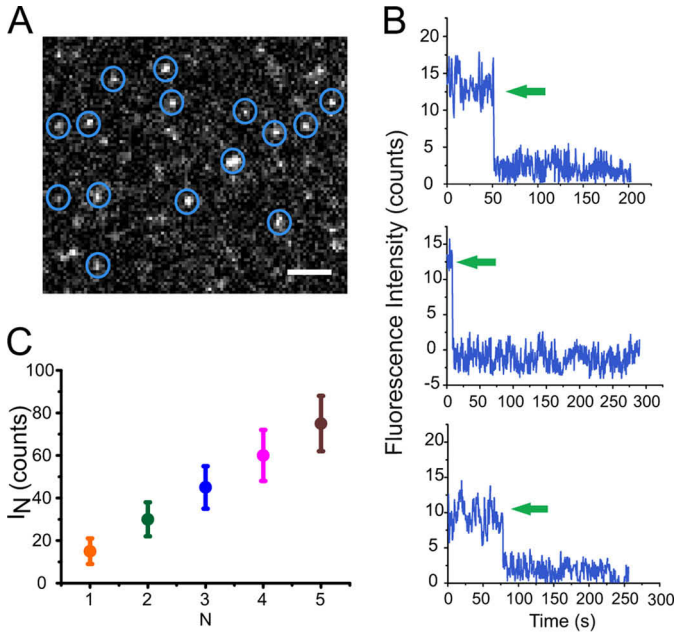

FIGURE 4. **Detection of single Alexa 555 fluorophores by TIRF microscopy.** *A,* TIRF image of single Alexa 555 molecules immobilized on a clean glass coverslip. *Scale bar*, 1 μm. Each particle was detected and the fluorescence intensity measured over time. *B,* the intensity of the particles that showed a single bleaching event were averaged over time and considered as the intensity of one single fluorophore. Some representative fluorescence intensity traces of individual Alexa 555 particles with a single bleaching event are shown in *blue*. The *green arrows* indicate the bleaching step. *C,* μ (mean fluorescence intensity) and σ (standard deviation) values were calculated for one (*orange*), two (*green*), three (*blue*), four (*magenta*), and five (*brown*) fluorophores. The μ and σ for a single fluorophore was determined from *B* and for 2–5 fluorophores was estimated according to the equation $\mu_N = N\mu_1 \pm N^{1/2}\sigma_1$ (1). *N* corresponds to the number of fluorophores. The *y* axis shows the fluorescence intensity (counts).

include them in the analysis due statistical limitations of the method. These results show that oligomerization of EqtII is very fast and suggest that membrane binding is likely the rate-limiting step in the sets of reactions leading to pore formation.

The temporal analysis of the distribution of EqtII-Al488 species on the cell surface indicates that not all possible oligomeric species are populated, but that there is an excess of tetramers and hexamers over trimers and pentamers (Fig. 5, *D–G*). Overall, we found that monomers decreased over time, whereas dimers increased. Furthermore, tetramers appeared quickly and stayed constant over time, whereas the number of hexamers increased in the first 30 s and then remained constant. These findings show that the spatiotemporal organization of EqtII on the host membrane is dynamic and evolves in a time frame comparable with cell death induction.

Based on these data, we modeled the process of EqtII assembly upon binding to the cell surface. We built a simple kinetic model of EqtII oligomerization based on ODEs for complex formation up to hexamers (Fig. 5*H* and "Experimental Procedures"). We considered all reactions reversible and we fitted the system of ODEs to the experimental data in Fig. 5, *D–G*. The best fit was obtained for a reaction scheme where EqtII first binds to the membrane as a monomer and, after forming dimers, oligomerization proceeds via dimer condensation. From the fitting, we obtained the kinetic constants for the forward and backward reactions of oligomerization (Fig. 5*I*). Interestingly, dimer dissociation is negligible suggesting that monomers are unstable in the membrane. Moreover, formation of tetramers is 1 order of magnitude faster than other condensation reactions, suggesting a higher stability for this structure.

The Pathway of EqtII Assembly Is Important for Toxicity—To assess the functional relevance of our findings, we carried out similar experiments with a mutant form of EqtII that is labeled with Al555 at the N-terminal helix involved in pore formation (EqtII-L26C-Al555). This version of EqtII has significantly reduced hemolytic activity but is still also able to kill cells (Fig. 1). The lower activity of this mutant might be a result of the lower ability to insert the N terminus, which might impair efficient protein oligomerization, as recently proposed (26). To compare the oligomerization dynamics of both EqtII mutants, we took images at 1, 5, 10, and 15 min after adding 140 nM EqtII-L26C-Al555 to COS-1 cells. This is the concentration and time frame under which the less active form EqtII-L26C-Al555 induces cell death. Under these conditions, the number of particles per area was comparable for both mutants. Moreover, differences in concentration between both mutants are not expected to have significant effects on the kinetics of oligomerization or the formation of complexes as suggested by Baker *et al.* (33).

Our analysis revealed the presence of a major population of dimers, accompanied by significant amounts of monomers, trimers, and tetramers at 1 min after adding the toxin to the cells (Fig. 6*A*). These results shows that oligomerization of EqtII-L26C-Al555 is slower than that of EqtII-Al488, in agreement with the longer times required to induce cell death. Also in this case, EqtII-L26C-Al555 existed in the membrane in multiple oligomeric forms. But importantly, the nature of the supramolecular organization of this less active mutant was distinct from the active form. In this case, all oligomeric states up to tetramers were detected, but not higher order structures, which indicates that this mutant has less ability to self-assemble.

Furthermore, the distribution of oligomeric forms also evolved with time on the cell surface in the case of the less active mutant of EqtII-L26C-Al555 (Fig. 6, *A–D*). However, in this case, ODEs mathematical modeling based on the experimental results supported a different assembly pathway based on sequential condensation of monomers (Fig. 6, *I–L*). We also tested whether alternative assembly mechanisms can explain our experimental results. In the case of EqtII-L26C-Al555, we forced dimer-dimer condensation to occur in the mathematical model by introducing a lower limit for the association rate constant k_4 (defined as in Fig. 6*I*). This way we made sure that dimers condensate at a rate constant of similar order of magnitude as for all other bimolecular reactions in the system. The modified fits showed a decreased goodness with a sum of squared residuals 10–20% higher than for the fit presented in Fig. 6, *I–L*. Moreover, tetramers showed a preferential dissociation into a monomer-trimer pair, whereas the association of such a pair into a tetramer became negligible compared with dimer-dimer association. Such a mechanism lacks of chemical plausibility and we therefore propose the sequential addition of monomers as the most plausible model for the oligomerization of EqtII-L26C-Al555.

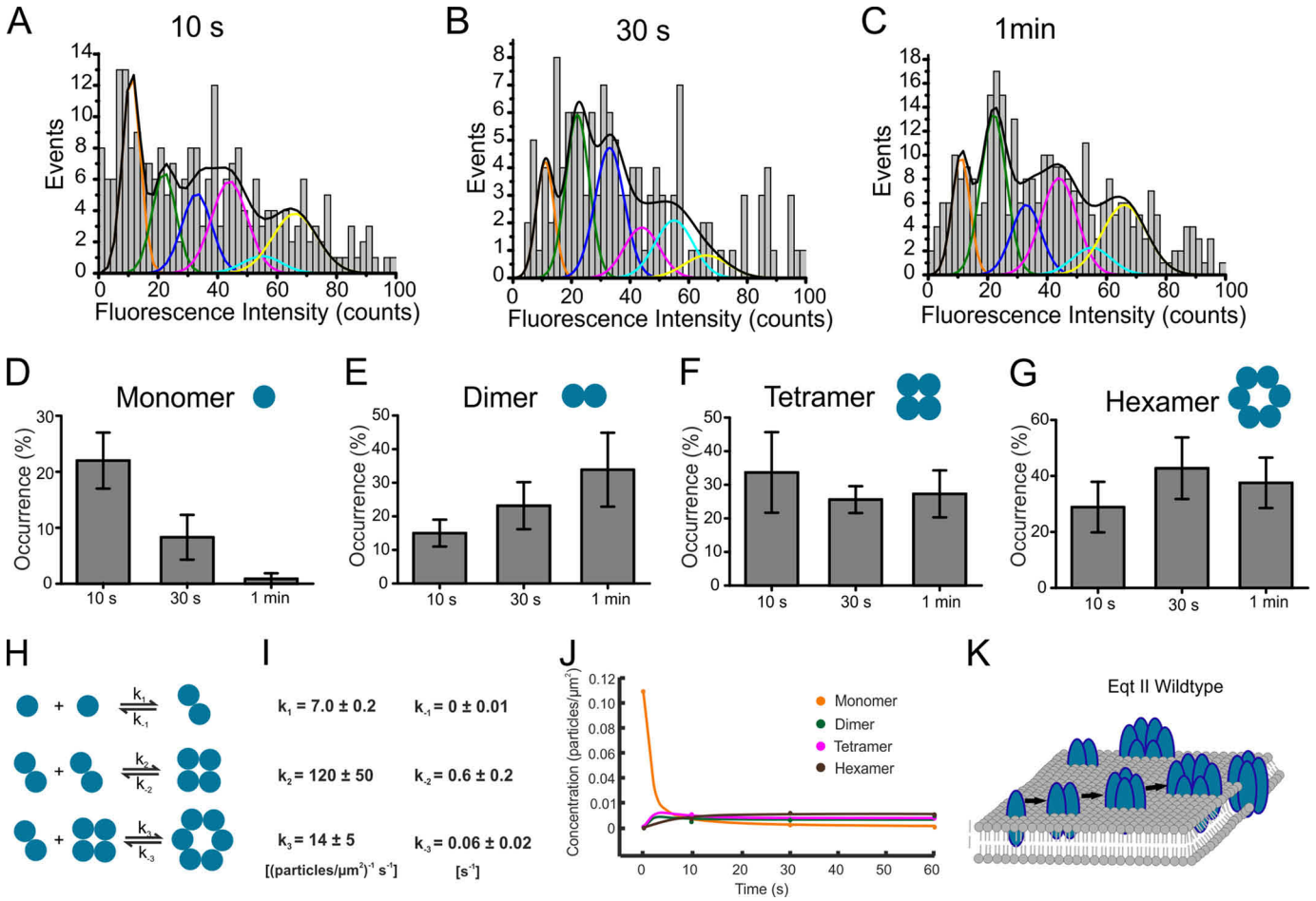

FIGURE 5. **EqtII-Al488 is present as a mixture of species that evolves with time.** *A–C*, intensity distribution of EqtII-Al488 on the cell surface at the indicated incubation times. For each condition, ~500 particles were analyzed. The resulting histograms were fitted with a sum of Gaussians to estimate the occurrence of monomers (*orange*), dimers (*green*), trimers (*blue*), tetramers (*magenta*), pentamers (*cyan*), and hexamers (*yellow*). *D-G*, temporal evolution of the distribution of EqtII-Al488 species on the cell surface. *Error bars* correspond to the error from the Gaussian fitting. *H*, kinetics of EqtII oligomerization analyzed by a simple mass action model. *I*, rate constants for the forward and backward reactions calculated by fitting to the experimental data. The errors represent the standard deviations of the three best fits. *J*, temporal evolution of the concentrations of EqtII monomers (*orange*), dimers (*green*), tetramers (*magenta*), and hexamers (*brown*) calculated from the model. The *circles* represent the experimental points. *K*, upon binding, EqtII oligomerizes on the plasma membrane via sequential condensation of dimers formed by monomer association. EqtII is present on the membrane as a mixture of species, whose distribution evolves with time and is close to equilibrium after 1 min of incubation.

When we investigated the dynamic behavior of the less active EqtII-L26C-Al555, we clearly found two populations with different mobility (Fig. 3, *D* and *F*): ~10% particles exhibited *apparent* Brownian diffusion, whereas the rest moved with *apparent* subdiffusion, best compatible with a model of confined diffusion (34). The corresponding *apparent* diffusion coefficients averaged for the free- and subdiffusing populations were 0.60 ± 0.01 and 0.36 ± 0.03 $\mu m^2/s$. Interestingly, the particles with *apparent* Brownian motion were low oligomeric forms of EqtII-L26C-Al555, formed by a mixture of monomers and dimers (Fig. 3*F*, *inset*). This suggests that the mobility of EqtII-L26C is reduced by oligomerization. Fig. 3, *G* and *H* (and supplemental Movie S1), shows an example of two diffusing EqtII-L26C-Al555 particles forming a complex. The two individual particles exhibit *apparent* free diffusion that becomes confined upon association. The brightness of the newly formed oligomer corresponds to the sum of the fluorescence intensity of the initial particles (Fig. 3*I*).

DISCUSSION

We have determined the spatiotemporal assembly of EqtII during its toxic action on the surface of living cells. Unlike most work so far with artificial model membranes, our data were obtained in the physiological environment of the target cell membrane and include conditions of equilibrium. Upon binding, we observed that EqtII rapidly initiates its oligomerization on the cell membrane. In contrast to previous assumptions that actinoporins are present exclusively as monomers and tetramers in the lipid bilayer (35), we found that EqtII clearly exists in the plasma membrane as a mixture of oligomeric species mostly including monomers, dimers, tetramers, and hexamers. These differences could be due to the different environments of the plasma membrane compared with pure lipid model membranes. Our data also suggest the presence of a small fraction of higher oligomers, which could be octamers and decamers. This mixture of oligomeric species is stable within the time range required for cell death. The results of the kinetic modeling fit best with oligomerization proceeding via the condensation of

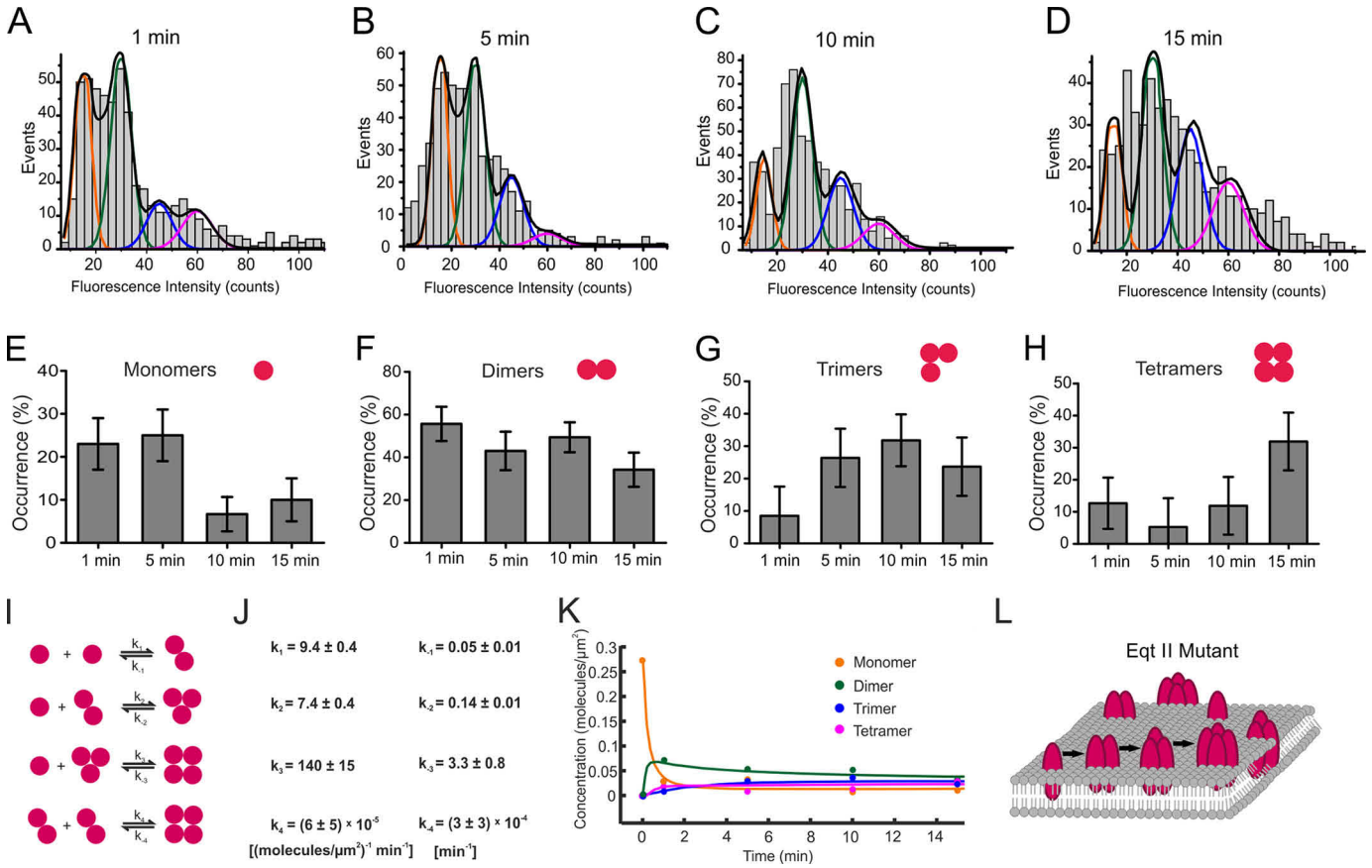

FIGURE 6. **The assembly mechanism is affected in the less active mutant EqtII-L26C-Al555.** *A–D*, intensity distribution of EqtII-L26C-Al555 on the cell surface at the indicated incubation times. For each condition, ~500 particles were analyzed. The resulting histograms were fitted with a sum of Gaussians to estimate the occurrence of monomers (*orange*), dimers (*green*), trimers (*blue*), and tetramers (*magenta*). *E–H*, temporal evolution of the distribution of EqtII-L26C-Al555 species on the cell surface. *Error bars* correspond to the error from the Gaussian fitting. *I*, the kinetics of EqtII oligomerization was analyzed by a simple mass action model. *J*, rate constants for the forward and backward reactions calculated by fitting to the experimental data. The errors represent the standard deviations of the three best fits. *K*, temporal evolution of the concentrations of EqtII monomers (*orange*), dimers (*green*), trimers (*blue*), and tetramers (*magenta*) calculated from the model. The *circles* represent the experimental points. *L*, upon binding, EqtII-L26C oligomerizes on the plasma membrane via sequential addition of monomers. It is present on the membrane as a mixture of species, whose distribution evolves with time and is close to equilibrium after 15 min of incubation.

dimer units that appear after the association of monomers in the membrane. This is in agreement with data for Sticholysin I, where forced dimerization by disulfide bonds increased pore activity (45).

Even though from our experimental data we cannot estimate what oligomeric state(s) would potentially be a functional unit for pore formation, mathematical modeling also suggests that tetramers are the most stable form of EqtII in the membrane, in agreement with recent determination of the stoichiometry of EqtII oligomers in supported bilayers (33), the structure of Sticholysin II in monolayers (13), and contrary to the models based on higher oligomeric species proposed for Fragaceatoxin C (15). However, one essential difference with structural studies reported so far is the detection of multiple coexisting oligomeric forms, which underscores the power of our single molecule approach when studying dynamic processes.

Importantly, an EqtII mutant with strongly reduced toxic activity also presents coexistence of species, but oligomerizes instead more slowly and up to tetramers via consecutive addition of monomers. Concretely, EqtII-L26C-Al555 contains a mutation in the N-terminal helix of the protein that likely hinders its membrane insertion and as a result reduces the efficiency of oligomerization (26). The results of the mathematical modeling suggest that it also lowers the stability of the dimer units compared with the active toxin. Furthermore, this mutation modifies the assembly pathway to sequential condensation of monomers. Altogether, our findings show that the molecular pathway of EqtII oligomerization is important for hemolytic activity and, therefore, protein function.

The analysis of EqtII mobility on the plasma membrane is typical of confined diffusion. This fits well with previous bulk fluorescence recovery after photobleaching data (6). Interestingly, in the case of the less active EqtII form, the single molecule approach allowed the detection of a small population of EqtII particles that diffuse freely, which interestingly corresponds to monomeric and dimeric forms of the toxin. This suggests that the confined diffusion observed for EqtII particles is due to the formation of larger oligomers, which would increase the likelihood of particle diffusion being affected by membrane crowding, interactions with the cytoskeleton and/or presence of raft-like domains (37, 38).

Based on the present results, we propose a model for the mechanism of EqtII toxic action on the target cells (Fig. 3*J*). Upon binding to the cell surface as a monomer, EqtII would

rapidly start oligomerizing and the first pore-forming oligomers would appear in a few seconds. EqtII would form first dimers by monomer association, and then further assemble via sequential addition of dimers in a set of reversible reactions. As a result, the proposed assembly mechanism would then give rise to a mixture of species on the cell surface that includes monomers, dimers, tetramers, and hexamers, as well as small fractions of higher oligomers, probably depending on toxin density on the membrane. In this model, we suggest that there might be more than one functional unit involved in the mechanism of pore formation of actinoporins. Notably, for both EqtII forms studied here, the distribution of species evolves over time and the accumulation of oligomers is linked to the time range required to attain cell death. This result might be linked with evidences obtained with EqtII and StI suggesting that pore assembly occurs via different functional states obtained by the successive incorporation of N-terminal α-helices to growing pores until a stable toroidal oligomeric structure is formed (26) (39). It is tempting to speculate that the coexistence of species is a general attribute of α-PFTs and a radical difference with respect to β-PFTs, which have been shown to assemble into a unique oligomeric form (29). This feature could be linked to the formation of pores lined by both lipids and proteins, also known as toroidal pores. In such architecture, the ability of the α-helices to induce lipid reorganization and stabilize the lipidic structure seems to be more important than the molecularity of the proteinaceous component of the functional units (40). Many α-PFTs, like actinoporins, the apoptosis regulators Bax and Bak, and a large number of antimicrobial peptides have been shown to form this type of pores (36, 41–43). Strikingly, the large number of coexisting species present in the membrane suggests that oligomers of different stoichiometry simultaneously contribute to membrane permeabilization. This may be a strategy of this kind of toxins to kill cells in a broad range of conditions (35) and is in line with a flexible pore structure, as recently shown for Bax and Bak (44). Importantly, our findings change the paradigm of how we understand membrane permeabilization by α-PFTs, so far focused on a unique oligomeric state as the predominant form of the toxin on the target membrane.

In summary, here we found that EqtII exists in the surface of the target cell as a dynamic mixture of multiple species. We propose a novel model for EqtII assembly that proceeds via the sequential condensation of dimer units. Moreover, EqtII toxicity was affected by altering the assembly mechanism, and therefore the oligomerization kinetics and the distribution of species on the cell surface, which supports the functional relevance of our findings.

Acknowledgments—We thank M. Zelman-Femiak, M. Axmann, and J. Langwoski for helpful discussions and the NIC from Heidelberg University for technical support. We are grateful to G. Anderluh for providing EqtII-L26C.

REFERENCES

1. Iacovache, I., van der Goot, F. G., and Pernot, L. (2008) Pore formation: an ancient yet complex form of attack. *Biochim. Biophys. Acta* **1778,** 1611–1623
2. Potrich, C., Tomazzolli, R., Dalla Serra, M., Anderluh, G., Malovrh, P., Macek, P., Menestrina, G., and Tejuca, M. (2005) Cytotoxic activity of a tumor protease-activated pore-forming toxin. *Bioconjug. Chem.* **16,** 369–376
3. Song, L., Hobaugh, M. R., Shustak, C., Cheley, S., Bayley, H., and Gouaux, J. E. (1996) Structure of staphylococcal α-hemolysin, a heptameric transmembrane pore. *Science* **274,** 1859–1866
4. Heuck, A. P., Tweten, R. K., and Johnson, A. E. (2001) Beta-barrel pore-forming toxins: intriguing dimorphic proteins. *Biochemistry* **40,** 9065–9073
5. Bayley, H. (2009) Membrane-protein structure: piercing insights. *Nature* **459,** 651–652
6. García-Sáez, A. J., Buschhorn, S. B., Keller, H., Anderluh, G., Simons, K., and Schwille, P. (2011) Oligomerization and pore formation by equinatoxin II inhibit endocytosis and lead to plasma membrane reorganization. *J. Biol. Chem.* **286,** 37768–37777
7. Hong, Q., Gutierrez-Aguirre, I., Barlic, A., Malovrh, P., Kristan, K., Podlesek, Z., Macek, P., Turk, D., Gonzalez-Manas, J. M., Lakey, J. H., and Anderluh, G. (2002) Two-step membrane binding by Equinatoxin II, a pore-forming toxin from the sea anemone, involves an exposed aromatic cluster and a flexible helix. *J. Biol. Chem.* **277,** 41916–41924
8. Kristan, K., Podlesek, Z., Hojnik, V., Gutiérrez-Aguirre, I., Guncar, G., Turk, D., González-Mañas, J. M., Lakey, J. H., Macek, P., and Anderluh, G. (2004) Pore formation by equinatoxin, a eukaryotic pore-forming toxin, requires a flexible N-terminal region and a stable β-sandwich. *J. Biol. Chem.* **279,** 46509–46517
9. Anderluh, G., Dalla Serra, M., Viero, G., Guella, G., Macek, P., and Menestrina, G. (2003) Pore formation by equinatoxin II, a eukaryotic protein toxin, occurs by induction of nonlamellar lipid structures. *J. Biol. Chem.* **278,** 45216–45223
10. Belmonte, G., Pederzolli, C., Macek, P., and Menestrina, G. (1993) Pore formation by the sea anemone cytolysin equinatoxin II in red blood cells and model lipid membranes. *J. Membr. Biol.* **131,** 11–22
11. Tejuca, M., Dalla Serra, M., Potrich, C., Alvarez, C., and Menestrina, G. (2001) Sizing the radius of the pore formed in erythrocytes and lipid vesicles by the toxin sticholysin I from the sea anemone *Stichodactyla helianthus*. *J. Membr. Biol.* **183,** 125–135
12. Groulx, N., McGuire, H., Laprade, R., Schwartz, J. L., and Blunck, R. (2011) Single molecule fluorescence study of the *Bacillus thuringiensis* toxin Cry1Aa reveals tetramerization. *J. Biol. Chem.* **286,** 42274–42282
13. Mancheño, J. M., Martín-Benito, J., Gavilanes, J. G., and Vázquez, L. (2006) A complementary microscopy analysis of Sticholysin II crystals on lipid films: atomic force and transmission electron characterizations. *Biophys. Chem.* **119,** 219–223
14. Mueller, M., Grauschopf, U., Maier, T., Glockshuber, R., and Ban, N. (2009) The structure of a cytolytic α-helical toxin pore reveals its assembly mechanism. *Nature* **459,** 726–730
15. Mechaly, A. E., Bellomio, A., Gil-Cartón, D., Morante, K., Valle, M., González-Mañas, J. M., and Guérin, D. M. (2011) Structural insights into the oligomerization and architecture of eukaryotic membrane pore-forming toxins. *Structure* **19,** 181–191
16. Schmidt, T., Schütz, G. J., Gruber, H. J., and Schindler, H. (1996) Local stoichiometries determined by counting individual molecules. *Anal. Chem.* **68,** 4397–4401
17. Meckel, T., Semrau, S., Schaaf, M. J., and Schmidt, T. (2011) Robust assessment of protein complex formation *in vivo* via single-molecule intensity distributions of autofluorescent proteins. *J. Biomed. Opt.* **16,** 076016
18. Jaqaman, K., Loerke, D., Mettlen, M., Kuwata, H., Grinstein, S., Schmid, S. L., and Danuser, G. (2008) Robust single-particle tracking in live-cell time-lapse sequences. *Nat. Methods* **5,** 695–702
19. Kusumi, A., Sako, Y., and Yamamoto, M. (1993) Confined lateral diffusion of membrane receptors as studied by single particle tracking (nanovid microscopy): effects of calcium-induced differentiation in cultured epithelial cells. *Biophys. J.* **65,** 2021–2040
20. Lee, G. M., Ishihara, A., and Jacobson, K. A. (1991) Direct observation of brownian motion of lipids in a membrane. *Proc. Natl. Acad. Sci. U.S.A.* **88,** 6274–6278
21. Qian, H., Sheetz, M. P., and Elson, E. L. (1991) Single particle tracking:

analysis of diffusion and flow in two-dimensional systems. *Biophys. J.* **60,** 910–921
22. Saxton, M. J., and Jacobson, K. (1997) Single-particle tracking: applications to membrane dynamics. *Annu. Rev. Biophys. Biomol. Struct.* **26,** 373–399
23. Calebiro, D., Rieken, F., Wagner, J., Sungkaworn, T., Zabel, U., Borzi, A., Cocucci, E., Zürn, A., and Lohse, M. J. (2013) Single-molecule analysis of fluorescently labeled G-protein-coupled receptors reveals complexes with distinct dynamics and organization. *Proc. Natl. Acad. Sci. U.S.A.* **110,** 743–748
24. Hoops, S., Sahle, S., Gauges, R., Lee, C., Pahle, J., Simus, N., Singhal, M., Xu, L., Mendes, P., and Kummer, U. (2006) COPASI: a COmplex PAthway SImulator. *Bioinformatics* **22,** 3067–3074
25. Anderluh, G., Barlic, A., Krizaj, I., Menestrina, G., Gubenšek, F., and Macek, P. (1998) Avidin-FITC topological studies with three cysteine mutants of equinatoxin II, a sea anemone pore-forming protein. *Biochem. Biophys. Res. Commun.* **242,** 187–190
26. Rojko, N., Kristan, K. Č., Viero, G., Žerovnik, E., Maček, P., Dalla Serra, M., and Anderluh, G. (2013) Membrane damage by an α-helical pore-forming protein, Equinatoxin II, proceeds through a succession of ordered steps. *J. Biol. Chem.* **288,** 23704–23715
27. Malovrh, P., Viero, G., Serra, M. D., Podlesek, Z., Lakey, J. H., Macek, P., Menestrina, G., and Anderluh, G. (2003) A novel mechanism of pore formation: membrane penetration by the N-terminal amphipathic region of equinatoxin. *J. Biol. Chem.* **278,** 22678–22685
28. Sergé, A., de Keijzer, S., Van Hemert, F., Hickman, M. R., Hereld, D., Spaink, H. P., Schmidt, T., and Snaar-Jagalska, B. E. (2011) Quantification of GPCR internalization by single-molecule microscopy in living cells. *Integr. Biol.* **3,** 675–683
29. Thompson, J. R., Cronin, B., Bayley, H., and Wallace, M. I. (2011) Rapid assembly of a multimeric membrane protein pore. *Biophys. J.* **101,** 2679–2683
30. Anderluh, A., Klotzsch, E., Reismann, A. W., Brameshuber, M., Kudlacek, O., Newman, A. H., Sitte, H. H., and Schütz, G. J. (2014) Single molecule analysis reveals coexistence of stable serotonin transporter monomers and oligomers in the live cell plasma membrane. *J. Biol. Chem.* **289,** 4387–4394
31. Cocucci, E., Aguet, F., Boulant, S., and Kirchhausen, T. (2012) The first five seconds in the life of a clathrin-coated pit. *Cell* **150,** 495–507
32. Xia, T., Li, N., and Fang, X. (2013) Single-molecule fluorescence imaging in living cells. *Annu. Rev. Phys. Chem.* **64,** 459–480
33. Baker, M. A., Rojko, N., Cronin, B., Anderluh, G., and Wallace, M. I. (2014) Photobleaching reveals heterogeneous stoichiometry for equinatoxin II oligomers. *ChemBioChem* **15,** 2139–2145
34. Wieser, S., and Schütz, G. J. (2008) Tracking single molecules in the live cell plasma membrane: do's and don't's. *Methods* **46,** 131–140
35. García-Ortega, L., Alegre-Cebollada, J., García-Linares, S., Bruix, M., Martínez-Del-Pozo, A., and Gavilanes, J. G. (2011) The behavior of sea anemone actinoporins at the water-membrane interface. *Biochim. Biophys. Acta* **1808,** 2275–2288
36. Landeta, O., Landajuela, A., Gil, D., Taneva, S., Di Primo, C., Sot, B., Valle, M., Frolov, V. A., and Basañez, G. (2011) Reconstitution of proapoptotic BAK function in liposomes reveals a dual role for mitochondrial lipids in the BAK-driven membrane permeabilization process. *J. Biol. Chem.* **286,** 8213–8230
37. Sackmann, E. (2014) Endoplasmatic reticulum shaping by generic mechanisms and protein-induced spontaneous curvature. *Adv. Colloid Interface Sci.* **208,** 153–160
38. Chappie, J. S., and Dyda, F. (2013) Building a fission machine: structural insights into dynamin assembly and activation. *J. Cell Sci.* **126,** 2773–2784
39. Antonini, V., Pérez-Barzaga, V., Bampi, S., Pentón, D., Martínez, D., Dalla Serra, M., and Tejuca, M. (2014) Functional characterization of sticholysin I and W111C mutant reveals the sequence of the actinoporin's pore assembly. *PloS One* **9,** e110824
40. Fuertes, G., Giménez, D., Esteban-Martín, S., Sánchez-Muñoz, O. L., and Salgado, J. (2011) A lipocentric view of peptide-induced pores. *Eur. Biophys. J.* **40,** 399–415
41. Valcarcel, C. A., Dalla Serra, M., Potrich, C., Bernhart, I., Tejuca, M., Martinez, D., Pazos, F., Lanio, M. E., and Menestrina, G. (2001) Effects of lipid composition on membrane permeabilization by sticholysin I and II, two cytolysins of the sea anemone *Stichodactyla helianthus*. *Biophys. J.* **80,** 2761–2774
42. Basañez, G., Sharpe, J. C., Galanis, J., Brandt, T. B., Hardwick, J. M., and Zimmerberg, J. (2002) Bax-type apoptotic proteins porate pure lipid bilayers through a mechanism sensitive to intrinsic monolayer curvature. *J. Biol. Chem.* **277,** 49360–49365
43. Qian, S., Wang, W., Yang, L., and Huang, H. W. (2008) Structure of transmembrane pore induced by Bax-derived peptide: evidence for lipidic pores. *Proc. Natl. Acad. Sci. U.S.A.* **105,** 17379–17383
44. Bleicken, S., Landeta, O., Landajuela, A., Basañez, G., and García-Sáez, A. J. (2013) Proapoptotic Bax and Bak proteins form stable protein-permeable pores of tunable size. *J. Biol. Chem.* **288,** 33241–33252
45. Valle, A., Lopez-Castilla, A., Pedrera, L., Martinez, D., Tejuca, M., Campos, J., Fando, R., Lissi, E., Alvarez, C., Lanio, M. E., Pazos, F., and Schreier, S. (2011) Cys mutants in functional regions of Sticholysin I clarify the participation of these residues in pore formation. *Toxicon* **58,** 8–17